

Resonant laser excitation and time-domain imaging of chiral topological polariton edge states

Damian Hofmann¹ and Michael A. Sentef^{1,2}

¹Max Planck Institute for the Structure and Dynamics of Matter,
Luruper Chaussee 149, 22761 Hamburg, Germany

²Institute for Theoretical Physics, University of Bremen, Otto-Hahn-Allee 1, 28359 Bremen, Germany
(Dated: June 17, 2022)

We investigate the dynamics of chiral edge states in topological polariton systems under laser driving. Using a model system comprised of topologically trivial excitons and photons with a chiral coupling proposed by Karzig *et al.* [Phys. Rev. X 5, 031001 (2015)], we investigate the real-time dynamics of a lattice version of this model driven by a laser pulse. By analyzing the time- and momentum-resolved spectral function, measured by time- and angle-resolved photoluminescence in analogy with time- and angle-resolved photoemission spectroscopy in electronic systems, we find that polaritonic states in a ribbon geometry are selectively excited via their resonance with the pump laser photon frequency. This selective excitation mechanism is independent of the necessity of strong laser pumping and polariton condensation. Our work highlights the potential of time-resolved spectroscopy as a complementary tool to real-space imaging for the investigation of topological edge state engineering in devices.

Light-matter interactions and nonequilibrium dynamics are unifying themes connecting solid state physics, quantum optics, and atomic and molecular physics. Photonic engineering in solids ranges from ultrafast dynamics in pump-probe spectroscopies^{1–3} via Floquet topological states^{4–14} and ultrafast modifications of interactions^{15–22} to cavity engineering of quantum materials with quantum light^{23–38}. These manipulations of matter with light usually involve the fermionic single-particle degrees of freedom. By contrast, in polaritonic systems often the description can be reduced to a purely bosonic theory, for example of polaritonic condensates³⁹. Here topological states^{40,41} have been proposed to exist in a variety of settings, including photonic systems^{42–45}, cold atoms in optical lattices^{46,47}, acoustic^{48–50} and mechanical^{51,52} systems. Recently polaritonic systems hosting chiral topological edge states were proposed theoretically^{53–55} and measured experimentally⁵⁶. However, for example in the work by Karzig *et al.*⁵³ the degree of control over the edge mode in terms of finetuning of relevant parameters was not discussed in much detail. In the experimental work by Klembt *et al.*⁵⁶ it was argued that the successful population and observation of chiral polariton edge modes was tied to the formation of a polariton condensate above a certain threshold power.

Here we show by calculations for a topological polariton lattice model how real-space imaging and time-resolved spectroscopy go hand-in-hand in demonstrating selective edge mode excitations by laser driving. We demonstrate that selective excitation of chiral edge modes is possible by laser pumping without the necessity of polariton condensation due to nonlinearities (i.e., without polariton-polariton interactions) if the pump laser frequency is tuned in resonance with the edge mode. A complementary real-space imaging reveals the edge localization of the populated modes.

Our setup is shown in Fig. 1. A quantum well (QW) harbors exciton modes that couple via dipole-dipole in-

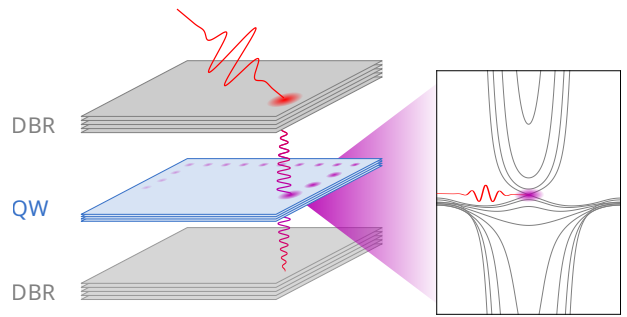
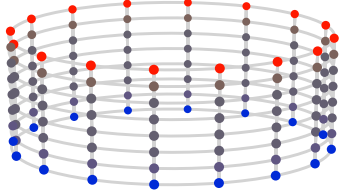


FIG. 1. Illustration of a semiconductor cavity setup. An isolated quantum well (QW) is placed between two optical dynamical Bragg reflectors (DBR). The cavity photon modes are populated by optical pumping and couple to excitonic states within the QW plane via dipole interaction. The specific coupling under consideration here yields topological edge states which can be selectively populated.

teractions to photon modes in a cavity, leading to the formation of exciton polaritons. As suggested for instance in Ref. 53 the QW could just as well be replaced by monolayer transition metal dichalcogenides⁵⁷. We will assume that there is a chiral coupling between excitons and polaritons⁵³.

For our calculations we start from a tight-binding model on a two-dimensional square lattice in a ribbon geometry, as shown in Fig. 2. Consider a lattice \mathcal{L} of size $N = N_x \times N_y$ with two bosonic modes at each site, representing photon and exciton populations, respectively. In the following, \hat{a}_i^0 (\hat{a}_i^1) denotes the photonic (excitonic) field operator at site i . Our model is a generalization of the Qi-Wu-Zhang model⁵⁸, also called half Bernevig-Hughes-Zhang model^{59,60}. We note that bosonic transport in a variation of this model including a non-linear interaction term has been studied by Weif⁶¹. The Hamil-

(a)



(b)

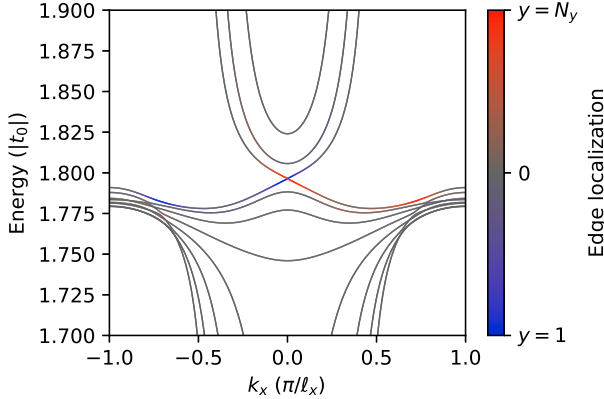


FIG. 2. (a) Real-space lattice structure of a ribbon with periodic boundary conditions in x and open boundary conditions in y direction. (b) Tight-binding topological polariton band structure of the resulting from the Hamiltonian \hat{H}_0 (2) on the ribbon geometry. The model parameters are $t_1 = 0.002|t_0|$, $g_0 = 0.2|t_0|$, $\varepsilon_0 = -4|t_0|$, and $\varepsilon_1 = -1.796|t_0|$, with an effective photon hopping $t_0 < 0$.

tonian has the form

$$\hat{H}(t) = \hat{H}_0 + \hat{F}(t) \quad (1)$$

with the static Hamiltonian

$$\hat{H}_0 = \sum_{i \in \mathcal{L}} \sum_{d \in \{0, d_x, d_y\}} \sum_{\alpha, \beta \in \{0, 1\}} t_{\alpha\beta}(d) \hat{a}_i^{\alpha\dagger} \hat{a}_{i+d}^{\beta} \quad (2)$$

where $i+d_\nu$ is the index of the nearest neighbor of site i in positive $\nu \in \{x, y\}$ direction. The hopping is determined by the matrices $\mathbf{t}(0) = \text{diag}(-\varepsilon_0, -\varepsilon_1)$ and

$$\mathbf{t}(d_x) = \begin{pmatrix} t_0 & ig_0/2 \\ ig_0/2 & t_1 \end{pmatrix}, \quad \mathbf{t}(d_y) = \begin{pmatrix} t_0 & g_0/2 \\ -g_0/2 & t_1 \end{pmatrix}. \quad (3)$$

Note that $\mathbf{t}(-d_\nu) = \mathbf{t}^\dagger(d_\nu)$ in order for \hat{H}_0 to be Hermitian. The parameters t_α are the photon and exciton hopping amplitudes, ε_α a constant energy offset, and g_0 the exciton-photon coupling strength. Assuming periodic boundary conditions in both x and y direction, H_0 can be written as

$$\hat{H}_0 = \sum_{\mathbf{k} \in \mathcal{L}'} \left(\begin{pmatrix} \hat{a}_{\mathbf{k}}^0 \\ \hat{a}_{\mathbf{k}}^1 \end{pmatrix}^\dagger \begin{pmatrix} \tau_0(\mathbf{k}) & g(\mathbf{k}) \\ g^*(\mathbf{k}) & \tau_1(\mathbf{k}) \end{pmatrix} \begin{pmatrix} \hat{a}_{\mathbf{k}}^0 \\ \hat{a}_{\mathbf{k}}^1 \end{pmatrix} \right). \quad (4)$$

Here, \mathcal{L}' denotes the discretized first Brillouin zone of the lattice,

$$\tau_\alpha(\mathbf{k}) = 2t_\alpha [\cos(\ell_x k_x) + \cos(\ell_y k_y)] - \varepsilon_\alpha \quad (5)$$

is the tight-binding dispersion, and

$$g(\mathbf{k}) = g_0 [\sin(\ell_x k_x) + i \sin(\ell_y k_y)] \quad (6)$$

is the momentum-dependent exciton-photon coupling where ℓ_x and ℓ_y denote the lattice spacing in the respective direction. The operators $\hat{a}_{\mathbf{k}}^\alpha = \frac{1}{\sqrt{N}} \sum_{j \in \mathcal{L}} e^{-i\mathbf{k} \cdot \mathbf{r}_j} \hat{a}_j^\alpha$ are obtained from the field operators by a discrete Fourier transform. The static Hamiltonian has a band structure that corresponds to a tight-binding approximation of the continuum model presented by Karzig et al.⁵³. The momentum-dependence of the coupling $g(\mathbf{k})$ leads to a non-zero Chern number $C_\pm = \mp 1$ of the upper (+) and lower (-) polariton band. The time-dependent driving is implemented by the operator

$$\hat{F}(t) = f_0 e^{-i\omega_d t} \hat{a}_{i_0}^{0\dagger} + \text{H.c..} \quad (7)$$

Here, for simplicity, the driving term acts directly only on the photonic mode $\alpha = 0$ at a single site i_0 which is located on the open side of the lattice boundary.

In order to show the presence of topological edge states in the system, we now add cylindrical boundary conditions, with periodic boundary conditions in x direction and open boundary conditions in y direction (Fig. 2a). The corresponding band structure obtained by a partial Fourier transform in x direction is shown in Fig. 2b.

Our simulations are performed in the semi-classical limit, where the bosonic operators are replaced by scalar complex fields. This corresponds to restricting the possible quantum states to the coherent states $|\psi\rangle$ parametrized by the scalar complex field $\psi \in \mathbb{C}^{2N}$, which satisfies $\hat{a}_i^\alpha |\psi\rangle = \psi_i^\alpha |\psi\rangle$. Since the Hamiltonian (1), including the driving term $\hat{F}(t)$, is of second order in the creation and annihilation operators, the coherent states are closed under the corresponding time evolution. Thus, if started in a coherent initial state, expectation values obtained from the semi-classical approach are exact. The equations of motion for the fields ψ_i^α are ($\hbar = 1$)

$$i\partial_t \psi_i^\alpha = \sum_{\substack{\beta \in \{0, 1\} \\ d \in \{0, \pm d_x, \pm d_y\}}} t_{\alpha\beta}(d) \psi_{i+d}^\beta + \delta_{i, i_0} \delta_{\alpha, 0} f_0 e^{-i\omega_d t} \quad (8)$$

for $(i, \alpha) \neq (i_0, 0)$. The initial state is chosen to be the coherent polaritonic vacuum state with $\psi_i^\alpha(0) = 0$ for all i and α .

In the semiclassical approximation, the double-time lesser Green's functions can be obtained directly from the fields as

$$\begin{aligned} G_{i\alpha; j\beta}^<(t_1, t_2) &:= -i \langle \hat{a}_j^{\beta\dagger}(t_2) \hat{a}_i^\alpha(t_1) \rangle \\ &= -i \psi_j^\beta(t_2) [\psi_i^\alpha(t_1)]^*. \end{aligned} \quad (9)$$

From the Green's functions, we compute the time-resolved spectral density⁶²

$$I(\omega, k) = \Im \iint dt_1 dt_2 S(t_1) S(t_2) e^{i\omega(t_1-t_2)} \tilde{G}^<(k; t_1, t_2) \quad (10)$$

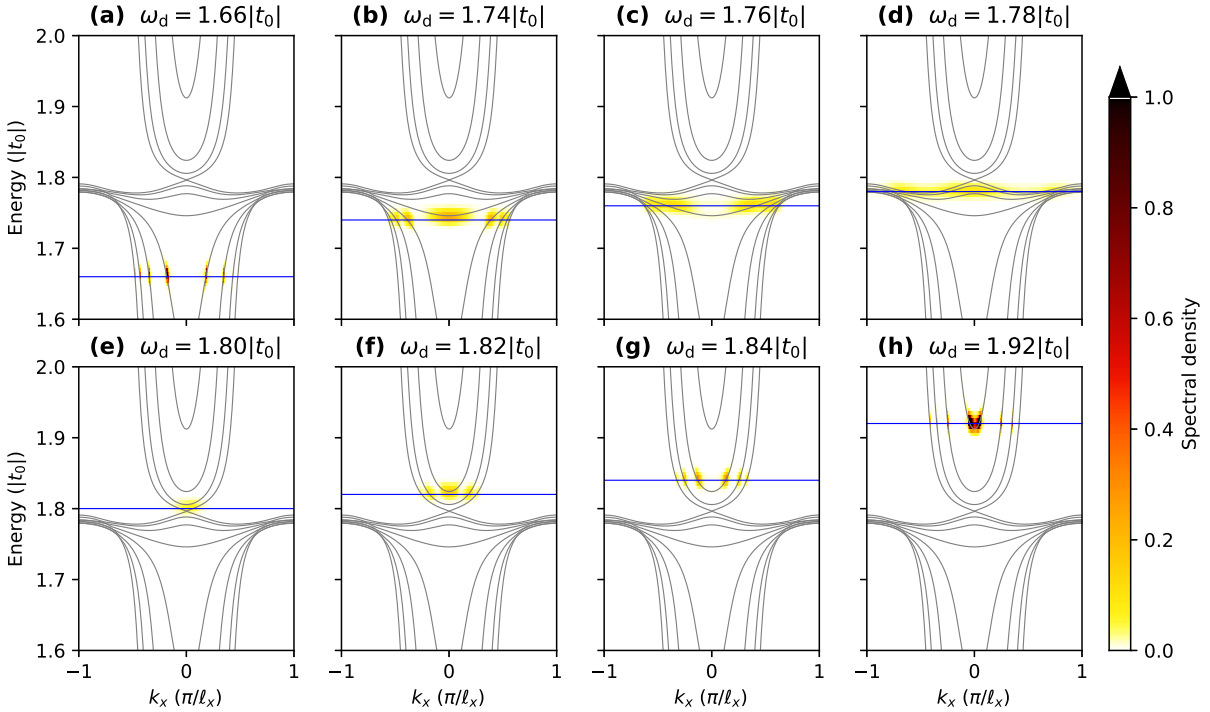


FIG. 3. (a)–(h) Time- and momentum-resolved spectral density [Eq. (10)] of the laser-irradiated system on a ribbon-shaped $N_x \times N_y = 256 \times 8$ lattice. The grey lines show the equilibrium band structure of the model (2). The driving frequency ω_d varies between subplots and is indicated by the blue line. The spectral density shows the excitation of the states resonant with the driving laser frequency. Here, the driving amplitude is $f_0 = 0.2|t_0|$ and the spectral density has been computed at a probe time of $t_p = 1600/|t_0|$ with $\sigma_p = 500/|t_0|$. The model parameters are the same as in Fig. 2.

with the probe shape $S(t) = \frac{1}{\sigma_p \sqrt{2\pi}} \exp\left(-\frac{(t-t_p)^2}{2\sigma_p^2}\right)$ where t_p is the probe time and σ_p the Gaussian width of the probe pulse. The reduced lesser Green's function used in Eq. (10) is given by

$$\tilde{G}^<(k; t_1, t_2) = \text{Tr}_{\alpha, y} \mathcal{F}_{x \rightarrow k} [G_{i_x, y, \alpha; i_x, y, \alpha}^<(t_1, t_2)] \quad (11)$$

which is Fourier-transformed along the periodic ribbon direction x and traced over y direction. We also trace here over the photon and exciton index, i.e., we compute the exciton-polariton spectral density. In principle, it is easily possible to resolve the spectral contributions of excitons and photons separately, but this will not be crucial for our analysis of edge localization of pumped modes below.

In Fig. 3 we present the time- and momentum-resolved spectral functions, mimicking time-domain photoluminescence spectra, of a continuously irradiated ribbon of size $N_x \times N_y = 256 \times 8$ with laser focused to a lattice site i_0 at the lower edge ($y = 0$) of the ribbon. The driving frequency of the external laser is varied to be below [Fig. 3(a-d)] the topological band gap, within the gap region [Fig. 3(e)], and above the gap [Fig. 3(g-h)]. As can be seen from the time-resolved spectral density, the polariton branches are selectively occupied by the resonant laser excitation, which shows that the external driving frequency is the main tuning knob for populating polarit-

ton branches in the absence of polariton-polariton interactions and associated mechanisms for polariton condensation.

Finally, we analyze in Fig. 4 the edge localization of the light-induced states through real-space analysis of the light-induced populations. Fig. 4(a) shows the localization at the lower edge, i.e., the ratio of intensity at $y = 1$ integrated (along the x direction) and the total intensity in the system at a given point in time. A clearly resonant resonant behavior is observed when the driving frequency matches the edge state energy of $\approx 1.8|t_C|$. The degree of localization is even more pronounced for the excitonic component of the polariton wavefunction. In Fig. 4(b) we analyze the localization integrated over the lower half $1 \leq y \leq 4$ of the ribbon, which consistently shows same the resonant behavior. In Fig. 4(c) we show representative real-space images for the photon and exciton densities in the on-resonance case. Here, besides the already discussed localization at the lower edge, one can also observe the chiral propagation of the edge mode from left to right as indicated by the arrow. By clear contrast, in Fig. 4(d) both the edge selectivity and chirality of the laser-pumped polariton populations are absent. These real-space images thus provide complementary information to the spectroscopic pictures presented in Fig. 3.

In summary we have shown lattice model simulations for the temporally and spatially resolved dynamics of

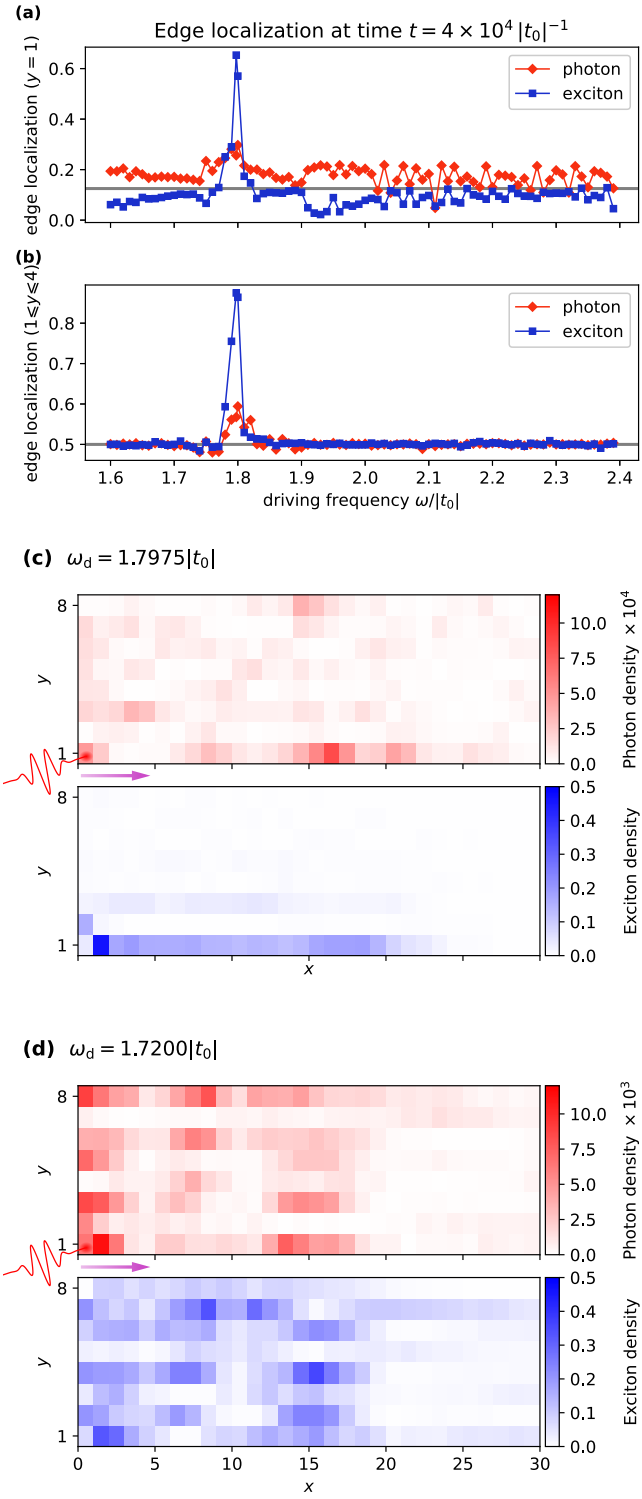


FIG. 4. (a)–(b) Fraction of the total population located at the lowest layer $y = 1$ (top panel) and within the lower half of the system $1 \leq y \leq 4$ (bottom panel). The horizontal grey lines indicate the fraction of the population located in the same region for a uniform distribution over the full 256×8 lattice. (c)–(d) Real-space density of the photon and exciton field at time $t = 1.2 \times 10^3 |t_0|^{-1}$ for resonant (panel c) and off-resonant (panel d) driving frequency. The driving field is localized at the bottom right corner of the displayed region. The direction of chiral propagation of the polariton modes is indicated by the purple arrow.

chiral topological exciton polaritons. We have demonstrated the selective excitation of chiral edge modes provided that the external driving frequency is sufficiently closely tuned to the topological band gap. An interesting open question pertains to the role of polariton-polariton interactions and the question of the importance of condensation versus resonant excitation for the experimentally observed chiral edge modes⁵⁶.

As an upshot from our calculations, it is straightforward to extend the formalism employed here to compute time-resolved spectroscopy in periodically driven many-body systems, both with continuous and ultrashort laser pulses. Specifically for continuous driving this is the realm of Floquet engineering^{63–66} of effective band structures, which is by itself a rapidly growing research field. The interface between the different fields of quantum simulators, nonequilibrium quantum materials science, and polaritonic condensates promises many interesting applications for future quantum technologies.

Acknowledgment. We acknowledge helpful discussions with G. Refael. We are particularly indebted to C. Bardyn for sharing his Gross-Pitaevskii simulation code. Financial support by the DFG through the Emmy Noether program (SE 2558/2-1) is gratefully acknowledged.

I. BIBLIOGRAPHY

- ¹ C. Giannetti, M. Capone, D. Fausti, M. Fabrizio, F. Parmigiani, and D. Mihailovic, *Advances in Physics* **65**, 58 (2016).
- ² D. N. Basov, R. D. Averitt, and D. Hsieh, *Nature Materials* **16**, 1077 (2017).
- ³ A. Cavalleri, *Contemporary Physics* **59**, 31 (2018).
- ⁴ T. Oka and H. Aoki, *Phys. Rev. B* **79**, 081406(R) (2009).
- ⁵ N. H. Lindner, G. Refael, and V. Galitski, *Nat Phys* **7**, 490 (2011).
- ⁶ T. Kitagawa, T. Oka, A. Brataas, L. Fu, and E. Demler, *Phys. Rev. B* **84**, 235108 (2011).
- ⁷ Y. H. Wang, H. Steinberg, P. Jarillo-Herrero, and N. Gedik, *Science* **342**, 453 (2013).
- ⁸ F. Mahmood, C.-K. Chan, Z. Alpichshev, D. Gardner, Y. Lee, P. A. Lee, and N. Gedik, *Nat Phys* **12**, 306 (2016).
- ⁹ G. Usaj, P. M. Perez-Piskunow, L. E. F. Foa Torres, and C. A. Balseiro, *Phys. Rev. B* **90**, 115423 (2014).
- ¹⁰ H. Dehghani, T. Oka, and A. Mitra, *Phys. Rev. B* **90**, 195429 (2014).
- ¹¹ M. A. Sentef, M. Claassen, A. F. Kemper, B. Moritz, T. Oka, J. K. Freericks, and T. P. Devereaux, *Nat Commun* **6**, 7047 (2015).
- ¹² M. Claassen, C. Jia, B. Moritz, and T. P. Devereaux, *Nature Communications* **7**, 13074 (2016).
- ¹³ H. Hübener, M. A. Sentef, U. D. Giovannini, A. F. Kemper, and A. Rubio, *Nature Communications* **8**, 13940 (2017).
- ¹⁴ J. W. McIver, B. Schulte, F.-U. Stein, T. Matsuyama, G. Jotzu, G. Meier, and A. Cavalleri, *Nature Physics* **16**, 38 (2020).
- ¹⁵ R. Singla, G. Cotugno, S. Kaiser, M. Först, M. Mitrano, H. Y. Liu, A. Cartella, C. Manzoni, H. Okamoto, T. Hasegawa, S. R. Clark, D. Jaksch, and A. Cavalleri, *Physical Review Letters* **115**, 187401 (2015).

- ¹⁶ C. Dutreix and M. I. Katsnelson, *Phys. Rev. B* **95**, 024306 (2017).
- ¹⁷ D. M. Kennes, E. Y. Wilner, D. R. Reichman, and A. J. Millis, *Nat Phys* **13**, 479 (2017).
- ¹⁸ M. A. Sentef, *Phys. Rev. B* **95**, 205111 (2017).
- ¹⁹ N. Tancogne-Dejean, M. A. Sentef, and A. Rubio, *Phys. Rev. Lett.* **121**, 097402 (2018).
- ²⁰ G. E. Topp, N. Tancogne-Dejean, A. F. Kemper, A. Rubio, and M. A. Sentef, *Nature Communications* **9**, 4452 (2018).
- ²¹ D. Golež, L. Boehnke, M. Eckstein, and P. Werner, *Phys. Rev. B* **100**, 041111(R) (2019).
- ²² M. Buzzi, D. Nicoletti, M. Fechner, N. Tancogne-Dejean, M. A. Sentef, A. Georges, M. Dressel, A. Henderson, T. Siegrist, J. A. Schlueter, K. Miyagawa, K. Kanoda, M.-S. Nam, A. Ardavan, J. Coulthard, J. Tindall, F. Schlawin, D. Jaksch, and A. Cavalleri, arXiv:2001.05389 [cond-mat] (2020), arXiv: 2001.05389.
- ²³ F. P. Laussy, A. V. Kavokin, and I. A. Shelykh, *Phys. Rev. Lett.* **104**, 106402 (2010).
- ²⁴ O. Cotlet, S. Zeytinoğlu, M. Sigrist, E. Demler, and A. Imamoğlu, *Phys. Rev. B* **93**, 054510 (2016).
- ²⁵ A. Kavokin and P. Lagoudakis, *Nature Materials* **15**, 599 (2016).
- ²⁶ D. Hagenmüller, J. Schachenmayer, S. Schütz, C. Genes, and G. Pupillo, *Phys. Rev. Lett.* **119**, 223601 (2017).
- ²⁷ M. A. Sentef, M. Ruggenthaler, and A. Rubio, *Science Advances* **4**, eaau6969 (2018).
- ²⁸ M. Rösner, R. E. Groenewald, G. Schönhoff, J. Berges, S. Haas, and T. O. Wehling, arXiv:1803.04576 [cond-mat] (2018), arXiv: 1803.04576.
- ²⁹ F. Schlawin, A. Cavalleri, and D. Jaksch, *Phys. Rev. Lett.* **122**, 133602 (2019).
- ³⁰ G. Mazza and A. Georges, *Phys. Rev. Lett.* **122**, 017401 (2019).
- ³¹ J. B. Curtis, Z. M. Raines, A. A. Allocata, M. Hafezi, and V. M. Galitski, *Phys. Rev. Lett.* **122**, 167002 (2019).
- ³² M. Kiffner, J. R. Coulthard, F. Schlawin, A. Ardavan, and D. Jaksch, *Phys. Rev. B* **99**, 085116 (2019).
- ³³ D. Hagenmüller, J. Schachenmayer, C. Genet, T. W. Ebbesen, and G. Pupillo, *ACS Photonics* **6**, 1073 (2019), arXiv: 1810.10190.
- ³⁴ A. A. Allocata, Z. M. Raines, J. B. Curtis, and V. M. Galitski, *Phys. Rev. B* **99**, 020504(R) (2019).
- ³⁵ V. Rokaj, M. Penz, M. A. Sentef, M. Ruggenthaler, and A. Rubio, *Phys. Rev. Lett.* **123**, 047202 (2019).
- ³⁶ S. Latini, E. Ronca, U. De Giovannini, H. Hübener, and A. Rubio, *Nano Lett.* **19**, 3473 (2019).
- ³⁷ M. Förög, L. Colombier, R. K. Patel, J. Lindlau, A. D. Mohite, H. Yamaguchi, M. M. Glazov, D. Hunger, and A. Högele, *Nature Communications* **10**, 1 (2019).
- ³⁸ A. Thomas, E. Devaux, K. Nagarajan, T. Chervy, M. Seidel, D. Hagenmüller, S. Schütz, J. Schachenmayer, C. Genet, G. Pupillo, and T. W. Ebbesen, arXiv:1911.01459 [cond-mat, physics:quant-ph] (2019), arXiv: 1911.01459.
- ³⁹ T. Byrnes, N. Y. Kim, and Y. Yamamoto, *Nature Physics* **10**, 803 (2014).
- ⁴⁰ M. Z. Hasan and C. L. Kane, *Rev. Mod. Phys.* **82**, 3045 (2010).
- ⁴¹ X.-L. Qi and S.-C. Zhang, *Rev. Mod. Phys.* **83**, 1057 (2011).
- ⁴² F. D. M. Haldane and S. Raghu, *Phys. Rev. Lett.* **100**, 013904 (2008).
- ⁴³ Z. Wang, Y. Chong, J. D. Joannopoulos, and M. Soljačić, *Nature* **461**, 772 (2009).
- ⁴⁴ M. C. Rechtsman, J. M. Zeuner, Y. Plotnik, Y. Lumer, D. Podolsky, F. Dreisow, S. Nolte, M. Segev, and A. Szameit, *Nature* **496**, 196 (2013).
- ⁴⁵ M. Hafezi, S. Mittal, J. Fan, A. Migdall, and J. M. Taylor, *Nature Photonics* **7**, 1001 (2013).
- ⁴⁶ G. Jotzu, M. Messer, R. Desbuquois, M. Lebrat, T. Uehlinger, D. Greif, and T. Esslinger, *Nature* **515**, 237 (2014).
- ⁴⁷ M. Aidelsburger, M. Lohse, C. Schweizer, M. Atala, J. T. Barreiro, S. Nascimbène, N. R. Cooper, I. Bloch, and N. Goldman, *Nature Physics* **11**, 162 (2015).
- ⁴⁸ Z. Yang, F. Gao, X. Shi, X. Lin, Z. Gao, Y. Chong, and B. Zhang, *Phys. Rev. Lett.* **114**, 114301 (2015).
- ⁴⁹ V. Peano, C. Brendel, M. Schmidt, and F. Marquardt, *Phys. Rev. X* **5**, 031011 (2015).
- ⁵⁰ R. Fleury, A. B. Khanikaev, and A. Alù, *Nature Communications* **7**, 11744 (2016).
- ⁵¹ L. M. Nash, D. Kleckner, A. Read, V. Vitelli, A. M. Turner, and W. T. M. Irvine, *PNAS* **112**, 14495 (2015).
- ⁵² R. Süssstrunk and S. D. Huber, *Science* **349**, 47 (2015).
- ⁵³ T. Karzig, C.-E. Bardyn, N. H. Lindner, and G. Refael, *Phys. Rev. X* **5**, 031001 (2015).
- ⁵⁴ A. V. Nalitov, D. D. Solnyshkov, and G. Malpuech, *Phys. Rev. Lett.* **114**, 116401 (2015).
- ⁵⁵ J. Yuen-Zhou, S. K. Saikin, T. Zhu, M. C. Onbasli, C. A. Ross, V. Bulovic, and M. A. Baldo, *Nature Communications* **7**, 11783 (2016).
- ⁵⁶ S. Klembt, T. H. Harder, O. A. Egorov, K. Winkler, R. Ge, M. A. Bandres, M. Emmerling, L. Worschach, T. C. H. Liew, M. Segev, C. Schneider, and S. Höfling, *Nature* **562**, 552 (2018).
- ⁵⁷ D. Xiao, G.-B. Liu, W. Feng, X. Xu, and W. Yao, *Phys. Rev. Lett.* **108**, 196802 (2012).
- ⁵⁸ X.-L. Qi, Y.-S. Wu, and S.-C. Zhang, *Phys. Rev. B* **74**, 085308 (2006).
- ⁵⁹ B. A. Bernevig, T. L. Hughes, and S.-C. Zhang, *Science* **314**, 1757 (2006), 17170299.
- ⁶⁰ J. K. Asbóth, L. Oroszlány, and A. Pályi, *A Short Course on Topological Insulators*, Lecture Notes in Physics No. volume 919 (Springer International Publishing, 2016) oCLC: 942849465.
- ⁶¹ T. Weiß, *Nonlinear Dynamics in Quantum Synchronization and Topological Transport*, PhD Thesis (Friedrich-Alexander-Universität Erlangen-Nürnberg, 2017).
- ⁶² J. K. Freericks, H. R. Krishnamurthy, and T. Pruschke, *Phys. Rev. Lett.* **102**, 136401 (2009).
- ⁶³ M. Bükov, L. D’Alessio, and A. Polkovnikov, *Advances in Physics* **64**, 139 (2015), publisher: Taylor & Francis eprint: <https://doi.org/10.1080/00018732.2015.1055918>.
- ⁶⁴ M. Holthaus, *J. Phys. B: At. Mol. Opt. Phys.* **49**, 013001 (2015), publisher: IOP Publishing.
- ⁶⁵ A. Eckardt and E. Anisimovas, *New J. Phys.* **17**, 093039 (2015), publisher: IOP Publishing.
- ⁶⁶ T. Oka and S. Kitamura, *Annual Review of Condensed Matter Physics* **10**, 387 (2019), eprint: <https://doi.org/10.1146/annurev-conmatphys-031218-013423>.